# Supporting Information

## Synergistic Upper Critical Solution Temperature–Lower Critical Solution Temperature Microgel-Hydrogel Composites for Bidirectional Thermoresponsive Smart Windows with Superior Optical Modulation and Dimensional Stability

*Jiaying Lei,[ǂ][a] Yuze Zhou,[ǂ][a] Yumeng Wang,[a] Yang Luo,[a] Xin Wang,[a] Yaocheng Yang,[a] Wei Ye,[a] Tengling Ye,*[a,c] Dongyan Tang *[a,b]*

[a] J. Lei, Y. Zhou, Y. Wang, Y. Luo, X. Wang, Y. Yang, W. Ye, Prof. T.Ye, Prof. D. Tang
School of Chemistry and Chemical Engineering, Harbin Institute of Technology, Harbin, China
[b] Prof. D. Tang
State Key Laboratory of Space Power-Sources, Harbin Institute of Technology, Harbin 150001, China
[c] Prof. T.Ye
State Key Laboratory of Photoelectric Conversion and Utilization of Solar Energy, Dalian Institute of Chemical Physics, Chinese Academy of Sciences, Dalian, 116023, Liaoning, China.
E-mail: dytang@hit.edu.cn; ytl@hit.edu.cn
ǂ these authors contributed equally to this work, * corresponding author

### Calculation formula

The integrated luminous transmittance $T_{lum}$ (380–780 nm), NIR transmittance $T_{NIR}$ (780-2500 nm), solar transmittance $T_{sol}$ (280-2500 nm) and corresponding transmittance modulations were calculated by Equations (1), (2), and (3), respectively:

$$T_{lum/NIR/sol} = \frac{\int \varphi_{lum/NIR/sol}(\lambda) T(\lambda) d\lambda}{\int \varphi_{lum/NIR/sol}(\lambda) d\lambda} \quad (1)$$

$$\Delta T_{lum/NIR/sol,low} = T_{lum/NIR/sol,\,24℃} - T_{lum/NIR/sol,\,4℃} \quad (2)$$

$$\Delta T_{lum/NIR/sol,high} = T_{lum/NIR/sol,24℃} - T_{lum/NIR/sol,40℃} \quad (3)$$

where $T(\lambda)$ denotes the recorded transmittance at a selected wavelength, $\varphi_{lum}(\lambda)$ is the standard luminous efficiency function for the photopic vision of human eyes (the wavelength range of 380–780 nm), $\varphi_{NIR/sol}$ is the NIR/solar irradiance spectrum for air mass 1.5G (wavelength coverage of 250–2500 nm,the sun standing 37° above the horizon, and solar zenith angle of 48.2° with 1.5-atmospherethickness). Due to the bidirectional optical features of PAM/PNM5 MGs smart window, the optical modulation capabilities at low temperature and high temperature were quantified with $\Delta T_{\mathrm{lum/NIR/sol,low}}$ and $\Delta T_{\mathrm{lum/NIR/sol,high}}$ respectively.

Table of contents

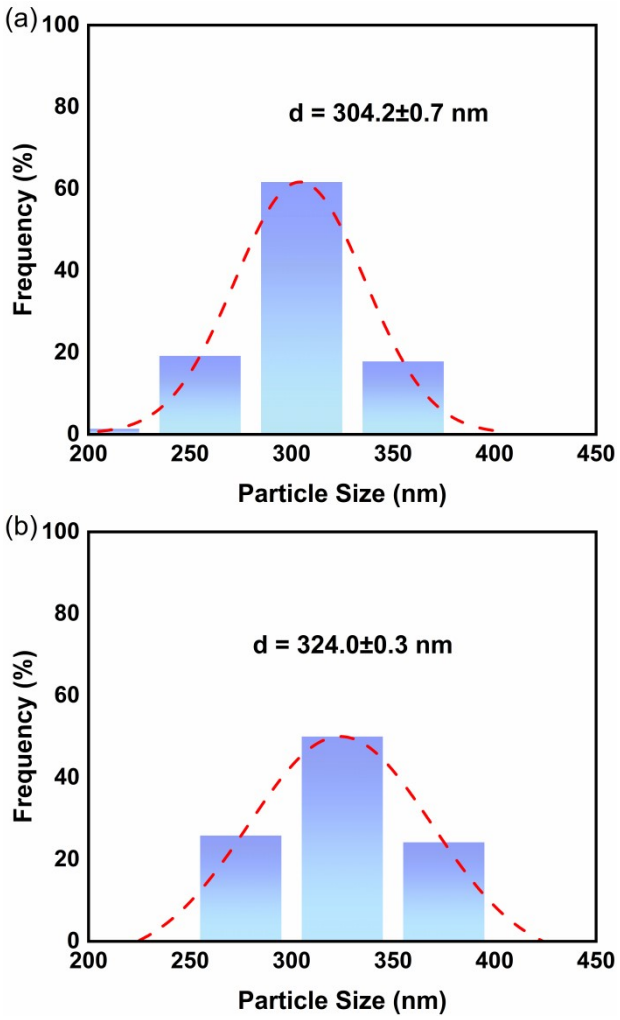


**Figure S1.** Histogram of particle size distribution of PNI MGs, PNM5 MGs, and PNM10 MGs.

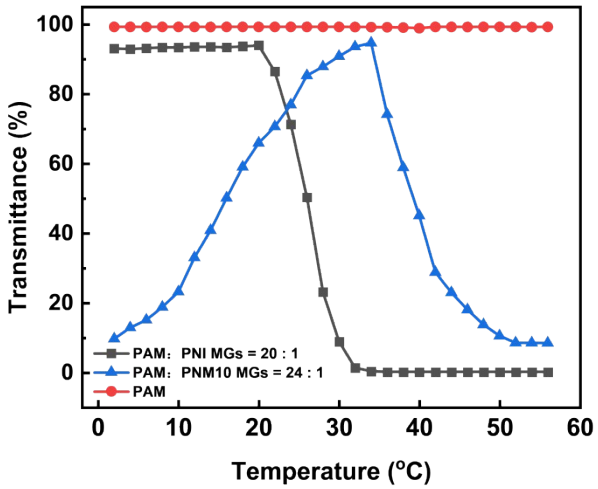


**Figure S2.** The transmittance curves of PAM: PNI MGs = 20:1 composite hydrogel, PAM: PNM10 MGs = 24:1 composite hydrogel and PAM hydrogel in the visible region (380–780 nm) at different temperatures.

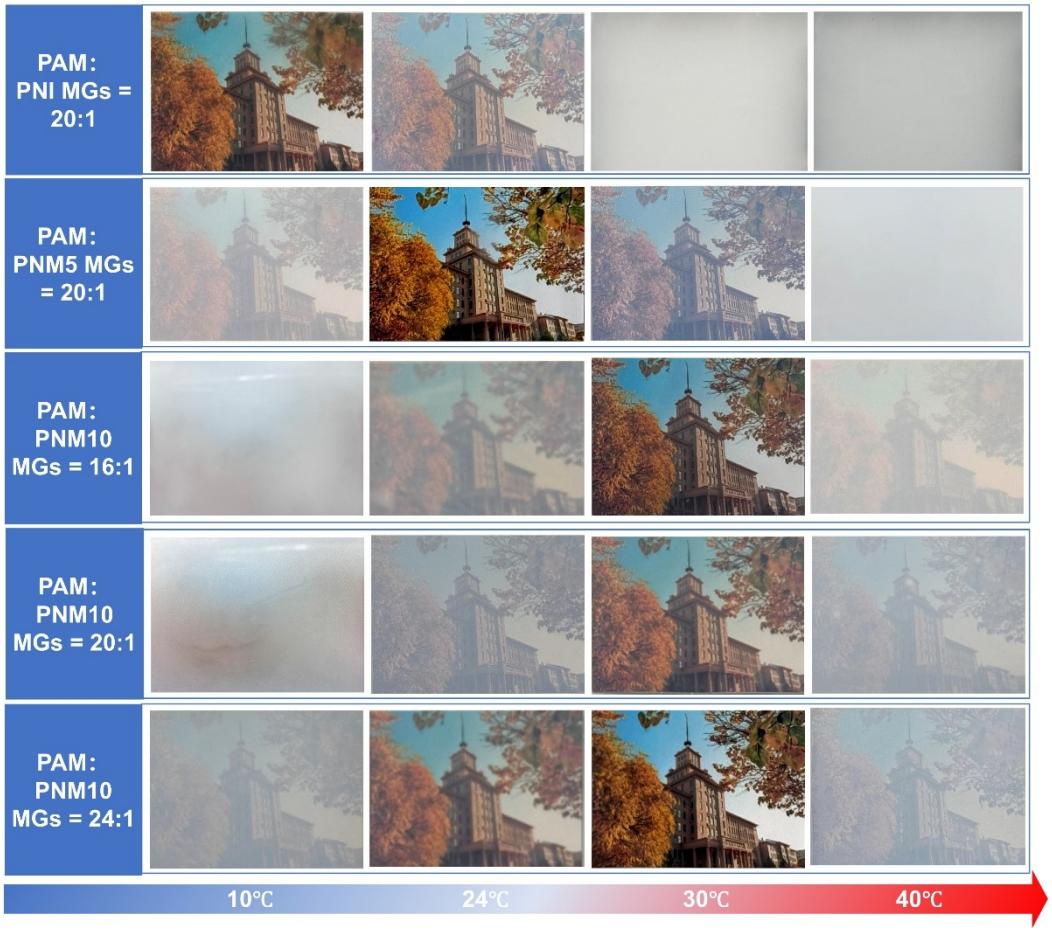


**Figure S3.** Optical images of composite hydrogels at different temperatures.


**Figure S4**. Response time test of PNIPAM hydrogel, PAM/PNM5 MGs composite Hydrogel and PNM5 MGs solution.

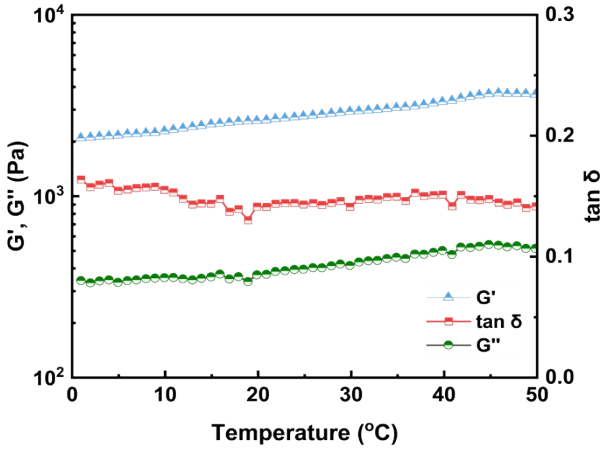


**Figure S5**. Temperature sweep spectra of $G'$, $G''$, and tan$\delta$ of PAM/PNM MGs composite hydrogel.

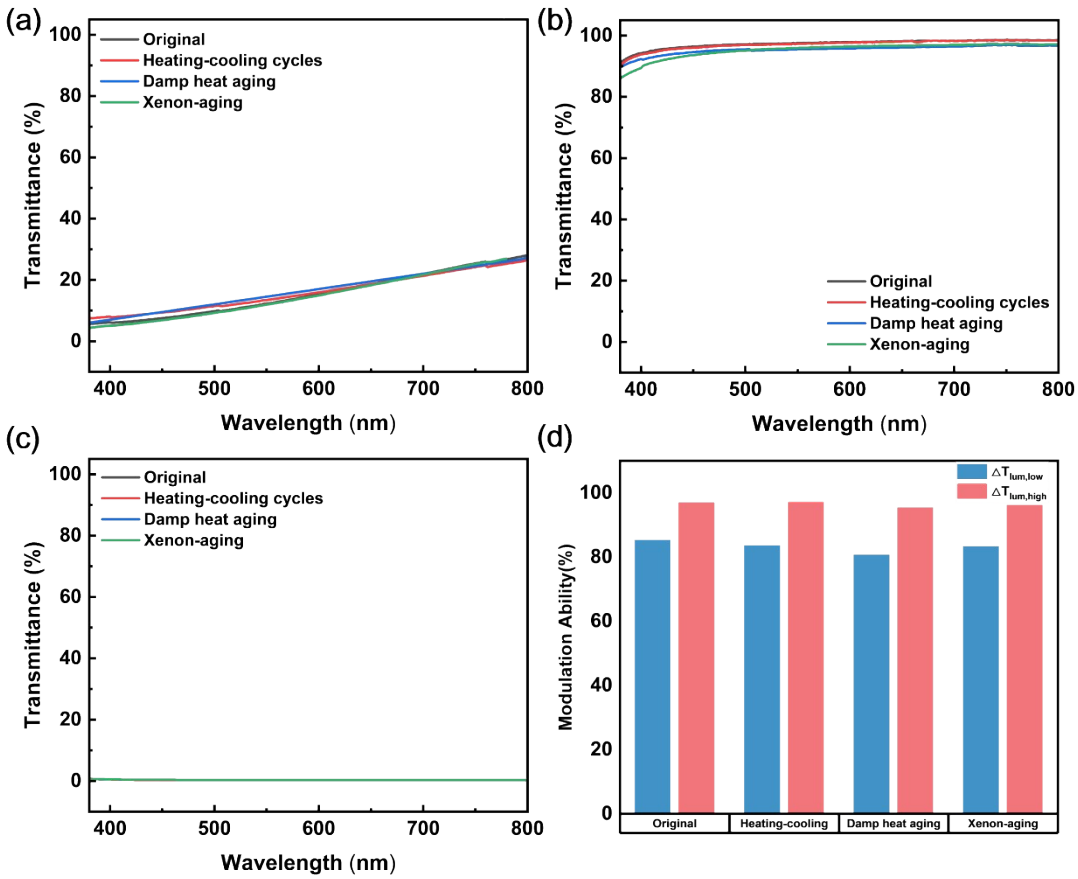


**Figure S6.** Optical stability and modulation efficiency of the PAM/PNM5 MGs composite hydrogel under various accelerated aging conditions at different temperatures. a) 4 °C, b) 24 °C, and c) 40 °C.

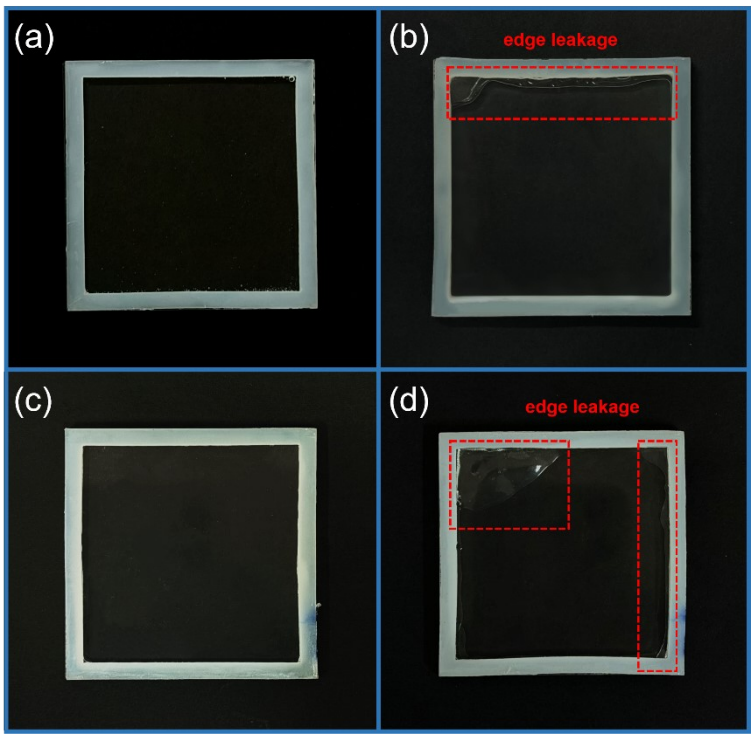


**Figure S7.** Dimensional stability of the smart window after aging. a) Original state. b) After 240 h of xenon-lamp aging. c) Original state. d) After 240 h of damp heat aging (85 °C, 85% RH).

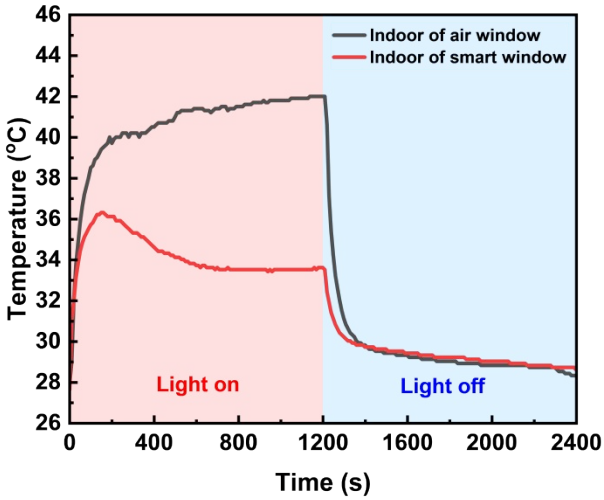


**Figure S8.** Time-dependent internal temperature changes of model houses with different windows in response to 200 mW $cm^{-2}$ xenon lamp irradiation.

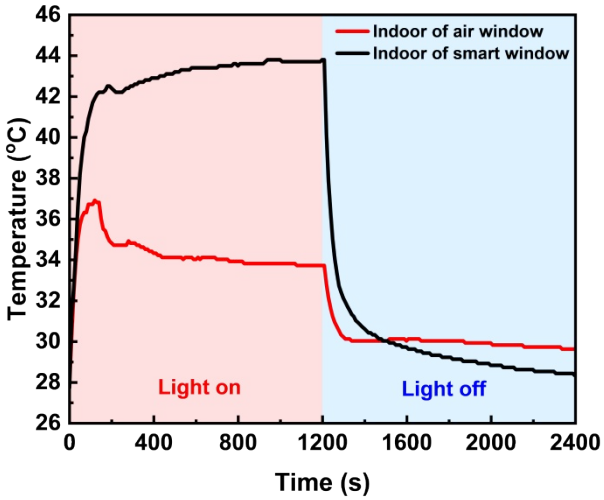


**Figure S9.** Time-dependent internal temperature changes of model houses with different windows in response to 300 mW $cm^{-2}$ xenon lamp irradiation.

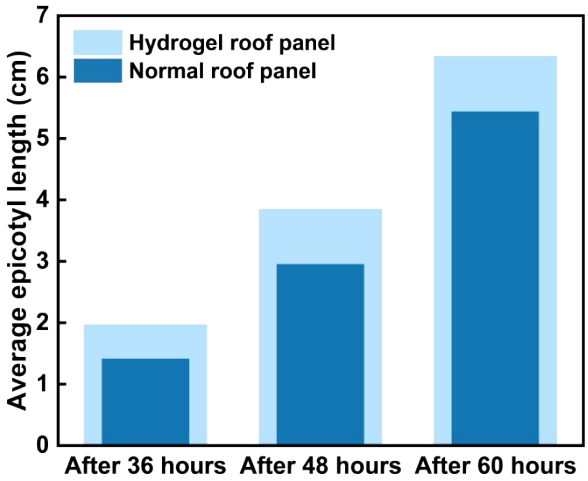


**Figure S10.** Epicotyl elongation in mung bean seedlings under hydrogel and normal roof panels.

**Table S1**. Optical properties of PAM/PNM5 MGs smart window.

| Sample | $T_{lum,4℃}$ (%) | $T_{NIR,4℃}$ (%) | $T_{sol,4℃}$ (%) | $T_{lum,24℃}$ (%) | $T_{NIR,24℃}$ (%) | $T_{sol,24℃}$ (%) | $T_{lum,40℃}$ (%) | $T_{NIR,40℃}$ (%) | $T_{sol,40℃}$ (%) |
|---|---|---|---|---|---|---|---|---|---|
| PAM/PNM 5 MGs | 11.78 | 25.06 | 17.99 | 96.97 | 57.73 | 78.43 | 0.06 | 1.46 | 0.01 |

| Sample | $\Delta T_{lum, low}$ (%) | $\Delta T_{NIR, low}$ (%) | $\Delta T_{sol, low}$ (%) | $\Delta T_{lum, high}$ (%) | $\Delta T_{NIR, high}$ (%) | $\Delta T_{sol, high}$ (%) |
|---|---|---|---|---|---|---|
| PAM/PNM5 MGs | 85.19 | 32.67 | 60.44 | 96.91 | 56.27 | 78.42 |

**Table S2**. Performances of representative smart windows in the literature

| Materials | $T_{lum}$ (%) | $\Delta T_{sol}$ (%) | Transition temperature (℃) | Stimuli | Ref. |
|---|---|---|---|---|---|
| PAM-Agar/PNIPAM/W-$VO_2$ composite hydrogel | 86.81 | 83.59 | 32.6 | Thermal | [1] |
| W-$VO_2$/PNIPAm-HPC hybrid hydrogel | 87.16 | 65.71 | 29 | Thermal | [2] |
| PNIPAm-AgNW mesh composite film | 78.3 | 58.4 | 31 | Thermal | [3] |
| PAAm-SDS-C18 | 99.05 | 33.42 | 20-50 | Thermal | [4] |
| Noncovalent crosslinked viscous PNIPAM GW solutions | 89.2 | 60.8 | 19.1-32.7 | Thermal | [5] |
| KCA/$Na_2SiO_3$/PNIPAm hydrogel | 87.37 | 69.65 | 27.2 | Thermal | [6] |
| P(AAm-*co*-AA) /NIPAm /AAm | 84.4 | 69.5 | 33.1-47.8 | Thermal | [7] |
| SDS/NaCl/PNIPAM-PAM | 80.3 | 47.2 | 24.9-32.4 | Thermal | [8] |
| PNIPAM/HPC/CMC-Gelatin(PHC-Gel) hydrogel | 95.2 | 57.2 | 20-35 | Thermal | [9] |
| HPC-PAM-PAA hydrogels | 88.7 | 53.9 | 30 | Thermal | [10] |
| HBPEC/PNIPAM hydrogel | 87.5 | 71.2 | 24.1-33.2 | Thermal | [11] |
| UCNPs@$SiO_2$-$NH_2$/PNIPAm hydrogel | 82.79 | 79.76 | 32 | Thermal | [12] |
| PAM/P(NIPAM-co-MAA5)(PAM/PNM5 MGs) | 96.97 | 78.42 | 26-38 | Thermal | This Work |

*N.M. not mentioned

## References


[1] H. Guan, Y. Lu, Y. You, S. Gao, L. Liu and G. Wu, *ACS Appl. Mater. Interfaces*, 2024, **16**, 52997–53006, DOI: 10.1021/acsami.4c13133.

[2] Y. Feng, W. Ma, H. Li, M. Yang, Y. Yu, S. Liu, X. Zeng, F. Huang, Y. Yang and Z. Li, *ACS Appl. Mater. Interfaces*, 2023, **15**, 5836–5844, DOI: 10.1021/acsami.2c19237.

[3] C. J. Lin, J. Hur, C. Y. H. Chao, G. Z. Liu, S. H. Yao, W. H. Li and B. L. Huang, *Sci. Adv.*, 2022, **8**, DOI: 10.1126/sciadv.abn7359.

[4] G. Xu, H. Xia, P. Y. Chen, W. She, H. N. Zhang, J. Ma, Q. S. Ruan, W. Zhang and Z. M. Sun, *Adv. Funct. Mater.*, 2022, **32**, 2109597, DOI: 10.1002/adfm.202109597.

[5] G. Li, J. W. Chen, Z. A. Yan, S. C. Wang, Y. J. Ke, W. Luo, H. R. Ma, J. G. Guan and Y. Long, *Mater. Horiz.*, 2023, **10**, 2004–2012, DOI: 10.1039/d3mh00057e.

[6] R. Guo, Y. Shen, Y. Chen, C. Cheng, C. Ye and S. Tang, *Chem. Eng. J.*, 2024, **486**, 150194, DOI: 10.1016/j.cej.2024.150194.

[7] W. Wang, K. Wang, Y. Cheng, C. Wu, R. Wu, J. Huang and Y. Lai, *Adv. Funct. Mater.*, 2024, 2413102, DOI: 10.1002/adfm.202413102.

[8] M. Dai, J. Zhao, Y. Zhang, H. Li, L. Zhang, Y. Liu, Z. Ye and S. Zhu, *ACS Appl. Mater. Interfaces*, 2022, **14**, 53314–53322, DOI: 10.1021/acsami.2c16319.

[9] L. Xie, X. Wang, X. Zou, Z. Bai, S. Liang, C. Wei, S. Zha, M. Zheng, Y. Zhou, O. Yue and X. Liu, *Small*, 2023, **19**, 2304321, DOI: 10.1002/smll.202304321.

[10] Y. C. Niu, Y. Zhou, D. X. Du, X. C. Ouyang, Z. J. Yang, W. J. Lan, F. Fan, S. S. Zhao, Y. P. Liu, S. Y. Chen, J. P. Li and Q. Xu, *Adv. Sci.*, 2022, **9**, 2105184, DOI: 10.1002/advs.202105184.

[11] M. Sun, H. Sun, R. Wei, W. Li, J. Lai, Y. Tian and M. Li, *Gels*, 2024, **10**, 494, DOI: 10.3390/gels10080494.

[12] J. Tian, H. Peng, X. Du, H. Wang, X. Cheng and Z. Du, *J. Alloys Compd.*, 2021, **858**, 157725, DOI: 10.1016/j.jallcom.2020.157725.